Supporting Information

Quasi-Solid-State Dye-Sensitized Solar Cells with Polymer Gel Electrolyte and Triphenylamine-Based Organic Dyes

*Jifu Shi , Shengjie Peng, Juan Pei, Yanliang Liang, Fangyi Cheng, Jun Chen**

Institute of New Energy Material Chemistry and Key Laboratory of Energy-Material Chemistry (Tianjin), Chemistry College, Nankai University, Tianjin 300071, People's Republic of China

*E-mail: chenabc@nankai.edu.cn

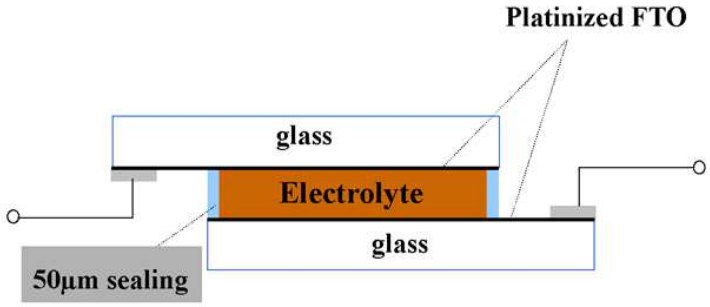

Figure S1. Schematic illustration of the electrochemical cell used for the measurement of diffusion limiting current of the polymer gel electrolyte.

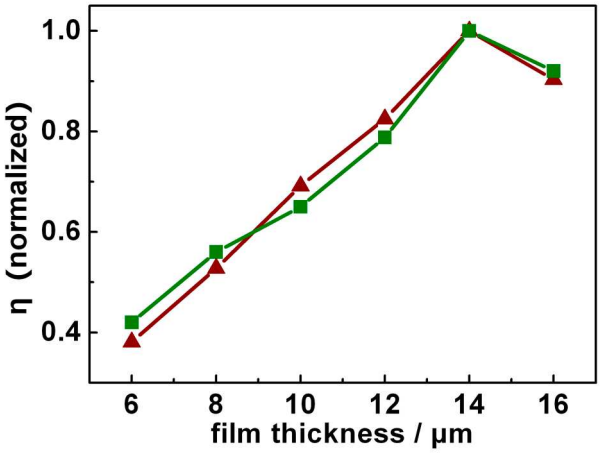

Figure S2. Normalized energy conversion efficiency of liquid-state solar cells sensitized by TPAR4 (red triangles) and TC4 (green squares) as a function of nanocrystalline TiO_2 film thickness. The electrolyte contained 0.6 M LiI, 0.06 M I_2 in the mixed solvent of EC/PC (with mass ratio of 8/2). The optimal thickness is 14 μm.

Effect of Dyes on the Photovoltaic Performance. Dyes also have important effect on the photovoltaic performance of quasi-solid-state DSCs. The photovoltaic performance of cell B is superior to that of cell A. The illumination intensity has stronger influence on the performance of cell B. Under the illumination intensity of 100 mW cm^{-2}, the η of cell B is 3.77 %. When the illumination intensity is decreased to 80 mW cm^{-2}, the η of cell B reaches to 4.71 %. An even higher efficiency of 5.76 % can be obtained upon reducing the light intensity to 30 mW cm^{-2}. At lower light level, the photocurrent is small, which decreases the mass-transfer-related losses in J_{sc} and FF and increases the conversion efficiency. For the cell A, the change of η as a function of light intensity is not as obvious as that of cell B because of its lower photocurrent even under the light intensity of 100 mW cm^{-2}.

The superior performance of cell B to cell A can be analyzed from the properties of the dye molecular. The lowest unoccupied molecular orbital (LUMO) level of the dye plays an important role in the determination of current flow in the electron injection process. The LUMO levels of TPAR4 and TC4 are -1.41 and -1.57 V vs NHE, respectively (1, 2). The more negative LUMO level can supply stronger driving force for effective electron injection. This is one of the reasons why the TC4-sensitized solar cell has higher J_{sc}.

On the other hand, for the cell B, the lower back reaction rate at the TiO_2/electrolyte interface between the injected electrons and I_3^- also results in higher J_{sc} as well as V_{oc} (3, 4). It can be seen from Figure 10b that the dark current for cell B occurs at higher forward bias than that of cell A, indicating that the sensitizer TC4 is more effective in retarding the back reaction than TPAR4, which is beneficial to increase the J_{sc} and V_{oc}. The different effect on suppressing the back reaction is partly caused by the different spatial array between the cyanoacrylic acid and rhodanine-3-acetic acid-based dyes on the TiO_2 surface (5, 6).

The Photovoltage Response. The different property of the dyes in retarding the back reaction can be examined by comparing the open-circuit voltage-decays (OCVD) curves of DSCs with different dyes. Figure S3 shows the decay of V_{oc} that follows after witching off the light (7). The decay of the photovoltage reflects the decrease in the density of electrons in the conduction band of the nanocrystalline TiO_2 particles. The electron density falls when the illumination is interrupted due to the back reaction between the injected electrons and I_3^- ions at the TiO_2/electrolyte interface. As shown in Figure S3, the decay of V_{oc} for cell B is slower than that of cell A, reflecting the excellent effect of TC4 on retarding the back reaction.

The electron lifetime (recombination time), τ, can be calculated from eq 3 (8, 9):

$$\tau = -\frac{k_B T}{e}\left[\frac{dV_{oc}}{dt}\right]^{-1} \qquad (3)$$

The results of electron lifetime as a function of V_{oc} are shown in the inset of Figure S3. The lifetime increases approximately exponentially with decreasing V_{oc}. The electron lifetime of the solar cells sensitized by different dyes increases in the order of TPAR4 < TC4.

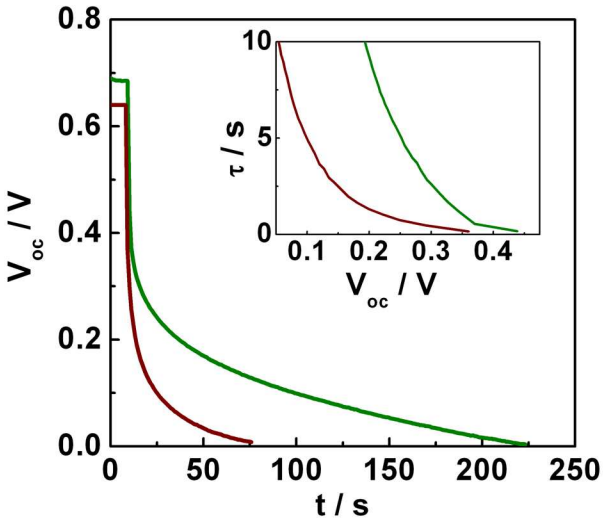

Figure S3. Open-circuit voltage-decays (OCVD) of cell A (red line) and cell B (green line) after switching off the light. The inset shows calculated electron lifetime vs V_{oc}.

Electrochemical Impedance Spectroscopy Analysis. The different effect of TPAR4 and TC4 on the photovoltaic performance can be explained in more detail in the EIS results measured in the dark at different forward biases. Figure S4 shows typical electrochemical impedance spectra of cell A and cell B measured at -0.7 V in the dark. The spectra show three arcs (10). The first (high frequency) semicircle represents the electron-transfer process at the platinum counter electrode. The second (intermediate frequency) arc corresponds to the charge-transfer at the TiO_2/electrolyte interface (11). The third (low frequency) arises from the diffusion of I_3^- in the electrolyte (12). It can be seen that the charge-transfer resistance at the TiO_2/electrolyte interface of cell B is larger than that of cell A, indicating that the electron recombination decreases with TC4 adsorption, which is in agreement with the dark current and OCVD results.

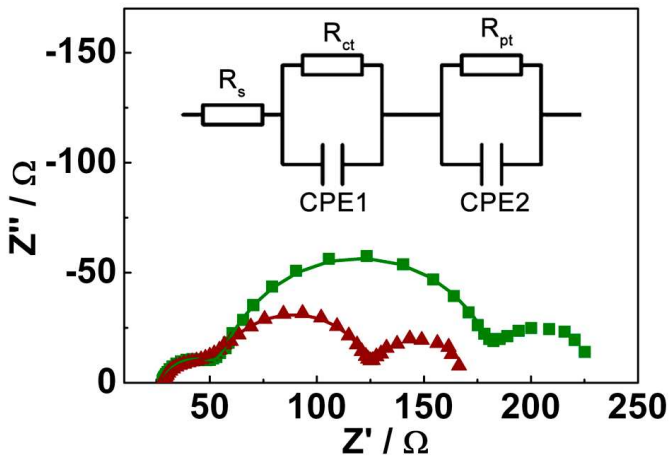

Figure S4. Electrochemical impedance spectra of cell A (red triangles) and cell B (green squares) measured in the dark at a forward bias of -0.7 V. The lines show the fitted results. The inset shows the equivalent circuit used for the curve fitting of the impedance spectra.

Fitting the high and intermediate frequency semicircles with the equivalent circuit $R_s(R_{ct}\text{CPE1})(R_{pt}\text{CPE2})$ shown in the inset of Figure S4 gives the corresponding electrokinetic parameters (13). Good agreement between the measured and the fitted data is achieved in all cases. In the equivalent circuit, R_s includes the resistance of the electrolyte, the FTO substrate, and the contact wires. R_{ct} is the charge-transfer resistance at the TiO_2/electrolyte interface. CPE1 represents the chemical capacitance produced by the accumulation of electrons in the TiO_2 film. The impedance of CPE is given by $Z_{CPE} = B(i\omega)^{-m}$, where ω is the angular frequency, B is the CPE parameter, and m ($0 \leq m \geq 1$) is the CPE exponent. For an ideal capacitance, the CPE exponent is 1 and in our experiments the CPE exponent is about 0.9, indicating that the deviation from an ideal capacitance is small (14). So the constant phase element CPE1 can be replaced by a capacitive element C_μ (14). Additionally, the electrochemical process at the electrolyte/Pt-FTO interface can be described by the charge-transfer impedance R_{pt} and the double layer capacitance CPE_2.

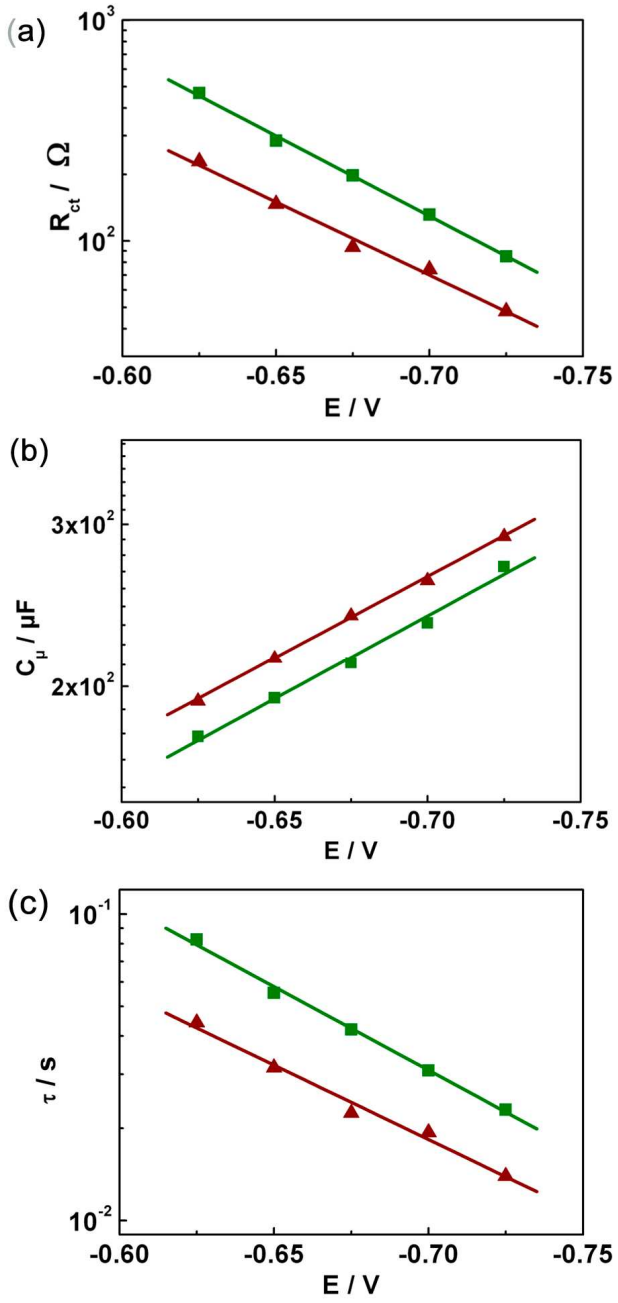

Figure S5. Fitting results of (a) charge transfer resistance (R_{ct}), (b) capacitance (C_μ), and (c) recombination time (τ) for cell A (red triangles) and cell B (green squares).

The fitting results of R_{ct} of cell A and cell B at different potentials are plotted in Figure S5a. The adsorption of TC4 on the surface of TiO_2 can more effectively reduce the number of recombination centers than that of TPAR4, leading to higher R_{ct} values for cell B. The C_μ values of the two cells are

presented in Figure S5b. C_μ follows a characteristic exponential rise with increasing forward bias given by (15):

$$C_\mu = C_a \exp\left[\frac{-\alpha e V}{k_B T}\right] + C_b \qquad (4)$$

where C_a is the prefactor of the exponential increase, V is the applied potential, C_b is the quasi-constant capacitance at low potentials, and α is a coefficient describing either the Boltzmann occupancy of the conduction band capacitance (α = 1) or an exponential distribution of trap states (α < 1) (15). In our measurements, α is calculated to be 0.106 for cell A and 0.107 for cell B. The coefficient α here are lower than that of the reported values (0.17-0.24) of DSCs with liquid-state electrolytes (15), which is probably caused by the difference of the polymer gel electrolyte with respect to liquid-state electrolytes. The C_μ values of cell B are lower than that of cell A mainly due to the negative shift of the conduction band edge (12). The difference of the potential at the same value of C_μ can indicate the shift of the conduction band edge (4, 11). As can be seen from Figure S5b, the adsorption of TC4 dye induces around 25mV negative shift of conduction band edge compared with TPAR4.

The values of V_{oc} for cell B are higher than that of cell A under various light intensities. The improvement of V_{oc} can therefore be ascribed to a combined effect of the negative shift of conduction band edge and the limitation of charge losses. The V_{oc} is determined by the difference between the quasi-Fermi level of TiO_2 and the potential of the redox couple in the electrolyte. The negative shift of the conduction band edge and the limitation of the charge losses increase the quasi-Fermi level of the conduction band electrons in the TiO_2 film and then increase the V_{oc} of cell B.

The electron lifetime τ can also be obtained by the product of R_{ct} and C_μ, $\tau = R_{ct} \times C_\mu$ (12). The τ of cell B is much larger than that of cell A (Figure S5c). This tendency is in keeping with that of Figure S3. The longer lifetime is one of the reasons why the photovoltaic performance of cell B is superior to that of the cell A. The increase in τ is associated with a pronounced rise in the charge-transfer resistance.

REFERENCES AND NOTES

(1) Liang, M.; Xu, W.; Cai, F.; Chen, P.; Peng, B.; Chen, J.; Li, Z. *J. Phys. Chem. C* **2007,** *111,* 4465–4472.

(2) Xu, W.; Peng, B.; Chen, J.; Liang, M.; Cai, F. *J. Phys. Chem. C* **2008,** *112,* 874–880.

(3) Ardo, S.; Meyer, G. J. *Chem. Soc. Rev.* **2009,** *38,* 115–164.

(4) Kuang, D.; Uchida, S.; Humphry-Baker, R.; Zakeeruddin, S. M.; Grätzel, M. *Angew. Chem. Int. Ed.* **2008,** *47,* 1923–1927.

(5) Tian, H.; Yang, X.; Chen, R.; Zhang, R.; Hagfeldt, A.; Sun, L. *J. Phys. Chem. C* **2008,** *112,* 11023–11033.

(6) Howie, W. H.; Claeyssens, F.; Miura, H.; Peter, L. M. *J. Am. Chem. Soc.* **2008,** *130,* 1367–1375.

(7) Brown, P.; Takechi, K.; Kamat, P. V. *J. Phys. Chem. C* **2008,** *112,* 4776–4782.

(8) Bisquert, J.; Zaban, A.; Greenshtein, M.; Mora-Seró, I. *J. Am. Chem. Soc.* **2004,** *126,* 13550–13559.

(9) Shankar, K.; Bandara, J.; Paulose, M.; Wietasch, H.; Varghese, O. K.; Mor, G. K.; LaTempa, T. J.; Thelakkat, M.; Grimes, C. A. *Nano Lett.* **2008,** *8,* 1654–1659.

(10) Jung, H. S.; Lee, J.-K.; Lee, S.; Hong, K. S.; Shin, H. *J. Phys. Chem. C* **2008,** *112,* 8476–8480.

(11) Wang, Q.; Ito, S.; Grätzel, M. Fabregat-Santiago, F.; Mora-Seró, I.; Bisquert, J.; Bessho, T.; Imai, H. *J. Phys. Chem. B* **2006,** *110,* 25210–25221.

(12) Fabregat-Santiago, F.; Bisquert, J.; Palomares, E.; Otero, L.; Kuang, D.; Zakeeruddin, S. M.; Grätzel, M. *J. Phys. Chem. C* **2007,** *111,* 6550–6560.

(13) Xu, W.; Pei, J.; Shi, J.; Peng, S.; Chen, J. *J. Power Sources* **2008,** *183,* 792–798.

(14) Hauch, A.; Georg, A. *Electrochim. Acta* **2001,** *46,* 3457–3466.

(15) Zhang, Z.; Zakeeruddin, S. M.; O'Regan, B. C.; Humphry-Baker, R.; Grätzel, M. *J. Phys. Chem. B* **2005**, *109,* 21818–21824.